Lab on a Chip

PAPER

View Article Online
View Journal | View Issue

Cite this: *Lab Chip*, 2021, **21**, 2574

Surface nanodroplet-based nanoextraction from sub-milliliter volumes of dense suspensions†

Jae Bem You, [ab] Detlef Lohse [b] and Xuehua Zhang *[ab]

Received 22nd February 2021,
Accepted 7th May 2021

DOI: 10.1039/d1lc00139f

rsc.li/loc

A greener analytical technique for quantifying compounds in dense suspensions is needed for wastewater and environmental analysis, chemical or bio-conversion process monitoring, biomedical diagnostics, and food quality control, among others. In this work, we introduce a green, fast, one-step method called nanoextraction for extraction and detection of target analytes from sub-milliliter dense suspensions using surface nanodroplets without toxic solvents and pre-removal of the solid contents. With nanoextraction, we achieve a limit of detection (LOD) of 10^{-9} M for a fluorescent model analyte obtained from a particle suspension sample. The LOD is lower than that in water without particles (10^{-8} M), potentially due to the interaction of particles and the analyte. The high particle concentration in the suspension sample, thus, does not reduce the extraction efficiency, although the extraction process was slowed down up to 5 min. As a proof of principle, we demonstrate the nanoextraction for the quantification of model compounds in wastewater slurry containing 30 wt% solids and oily components (*i.e.* heavy oils). The nanoextraction and detection technology developed in this work may be used in fast analytical technologies for complex slurry samples in the environment, industrial waste, or in biomedical diagnostics.

1 Introduction

Sample pretreatment is one of the most polluting steps in chemical analysis.[1] In particular, concentrating analytes with an extremely low concentration often requires a large amount of toxic solvents and multiple steps of operation with high energy input for separation such as high speed centrifugation. Waste chemicals are costly to dispose of safely and sometimes pose serious issues to our ecosystem. It is estimated that about 34 million liters of solvent waste are generated annually from liquid chromatography alone, without taking into account the solvent waste produced from sample pretreatment.[2] With the goal of developing sustainable technologies in mind, the solvent waste during sample pretreatment should be minimized.

Development of green analytical techniques for quantifying traces of compounds from suspensions with high solid concentration of particles is of broad interest in determining environmental pollutants in soil or water,[3] in process monitoring of fermentation or biomass conversion,[4,5] in biomedical diagnostics,[6–8] and in food quality control.[9,10] For example, quantification of harmful pesticides (*e.g.* organophosphates) or pharmaceutical drugs from drinking water treatment sludge is crucial for determining proper disposal procedures.[11] Detection of harmful toxins like cereulide (a type of depsipeptide) or aflatoxin B_1 (one of the most dangerous mycotoxins) from food is compulsory to safeguard the public health against foodborne illnesses.[12,13]

Presently, removal of solid contents in such suspension samples prior to analysis of target compounds is required to guarantee high detection sensitivity and to prevent deterioration of analytical instruments, in particular clogging the capillary column in a chromatography system.[14] Therefore, development of green analytical technology is needed to simplify the analysis of slurry samples. Specifically, a technology that produces minimal waste and uses non-harmful solvents, as outlined in the 12 principles of green analytical chemistry (GAC),[15] is highly desirable.

Currently, solids in suspension samples are mostly removed by centrifugation or filtration. Although these standard methods are simple, some intrinsic limitations hinder efficient and fast extraction from suspensions with high solid contents. First of all, removal of small particles (*i.e.* <1 μm) requires high power consumption by using specialized centrifugation equipment.[16,17] Second, clogging of filter pores by the particles is a common issue during filtration,[18,19] potentially producing unnecessary waste.

[a] *Department of Chemical and Materials Engineering, University of Alberta, Alberta T6G 1H9, Canada. E-mail: xuehua.zhang@ualberta.ca*
[b] *Physics of Fluids Group, Max Planck Center Twente for Complex Fluid Dynamics, JM Burgers Center for Fluid Dynamics, Mesa+, Department of Science and Technology, University of Twente, Enschede 7522 NB, The Netherlands*

† Electronic supplementary information (ESI) available: Schematic diagram showing the steps for operating the portable nanoextraction device; plots showing the influence of exposure time on background Nile red fluorescence intensity; limit of detection for the Rhodamine B dye. See DOI: 10.1039/d1lc00139f

Third, certain target compounds may adsorb on the filter surface reducing extraction efficiency. For instance, pesticides – many of which are hydrophobic – are prone to adsorb on the surface of filter membranes.[20,21] Undesired adsorption can lead to the loss of analytes during filtration before detection.[22–24] For instance, Ahmad *et al.* reported up to 95% loss of pesticide analyte from water after syringe filtration.[24] Finally, both filtration and centrifugation in the sample pretreatment are not applicable to *in situ* analysis of target compounds. An approach to separate, extract and concentrate the analytes directly from slurry samples without removal of solids is needed to significantly simplify and speed up the analysis of slurries containing high concentration of solids.

Enriching traces of target compounds by extraction is an effective way of improving detection sensitivity.[25,26] Various forms of extraction have been demonstrated including use of porous membranes in extraction driven by an electric field,[27–30] formation of tiny extractant droplets generated by ultrasonication for liquid phase extraction,[31,32] or use of nanoparticles as sorbents in solid phase extraction.[33,34] In particular, liquid–liquid extraction by using extractant microdroplets can reach high extraction efficiency, due to efficient mass transfer enabled by the high surface area-to-volume ratio of small droplets.[35] Approaches such as the single-drop microextraction[35,36] or bubble-in-drop microextraction[37,38] use a single extractant droplet hanging at the tip of a syringe needle immersed in the sample solution to extract the target compounds.

The simple setup also enables *in situ* analysis in tandem with analytical instruments such as a UV–vis spectrometer.[39,40] However, the single drop extraction is not compatible with slurry samples as the droplet can easily detach from the needle upon collision with the particles or from the high shear stress generated during the stirring motion.[41] Although the droplet can be protected with a hollow fiber membrane,[41,42] blockage and fouling of pores by the particles can occur and lower the extraction performance.[43]

Recently, many studies have applied dispersive liquid–liquid microextraction (DLLME) to extract and detect chemicals from various types of samples, including body fluids,[7,8] foods,[10,44,45] or environmental samples.[46,47] In a typical DLLME process, extractant microdroplets form spontaneously by mixing an extractant solution with an aqueous sample.[48] Similar to single drop microextraction, target compounds in the mixture are readily extracted into the extractant microdroplets according to the high partition coefficient in the droplets. The extractant droplets need to be separated from the mixture and collected using a centrifuge. Despite its excellent extraction efficiency and simplicity, DLLME is not suitable for *in situ* extraction and analysis of target compounds in solid suspensions as additional filtration or centrifugation steps are required to remove the solid contents from the sample prior to the extraction procedure. Moreover, environmentally harmful extractants such as halogenated hydrocarbons (*e.g.* chloroform) are often used.[49,50]

To overcome these drawbacks of DLLME, surface nanodroplets provide an effective approach for liquid–liquid extraction. Surface nanodroplets are droplets on solid surfaces with less than 100 nm in height and sub-femtoliter in volume.[51] Extensive research has shown that surface nanodroplets can be simply produced by a solvent exchange process in a controlled way.[52–56] Li *et al.* formed the surface nanodroplets to extract target analytes by flowing the sample solution over the droplets in the same chamber.[57,58] *In situ* analysis was possible as the nanodroplets are pinned on a substrate during the extraction process. The droplet component was controlled with the solutions used for solvent exchange. Extraction with surface nanodroplets – *i.e.* nanoextraction – also avoids excessive use of chemicals by minimizing the volume of extractant oils and solvents during sample pre-treatment, enabling an eco-friendly analytical technology.

To date, nanoextraction has not been applied in analyte concentration from slurries. It remains unclear how solids affect the droplet stability and extraction efficiency and rate. In this work, we employ surface nanodroplets to extract and detect compounds from high-solid suspensions – with a solid content up to 30 wt% – without pre-removal of the solids. Through *in situ* detection of a model compound from suspension samples, we find that the final extraction outcome with surface nanodroplets is not influenced by the solid concentration, although the particles may slow down initially due to their adsorption at the droplet interface. As a proof-of-concept, we demonstrate the extraction and detection of target analytes from industrial waste slurry. The approach reported in our work facilitates and speeds up the pre-treatment of suspension samples by enabling one-step extraction of target analytes. This novel method may be applicable to extraction and analysis of high-solid suspensions in various fields such as environmental monitoring or food quality control.

2 Experimental

2.1 Hydrophobization of glass capillaries for nanodroplet formation

The surface of glass capillary tubes (Kimble Products, Inc., USA) with an inner diameter of 1.1–1.4 mm, outer diameter of 1.5–1.8 mm, and length of 100 mm was made hydrophobic using octadecyltrichlorosilane (OTS) (Sigma Aldrich) by following the protocol reported in ref. 59. Briefly, the glass capillaries were cleaned with a piranha solution composed of 70% H_2SO_4 (Fisher Scientific) and 30% H_2O_2 (Fisher Scientific) (v/v) for 15 min at 75 °C. After cleaning, the capillary tubes were sonicated in water and then in ethanol for 5 min each before drying with a stream of air. Subsequently, the capillary tubes were immersed in an amber bottle containing 100 mL of hexane (Sigma Aldrich) and 100 μL of OTS. The bottle was tightly closed and kept at room

temperature (20.5 °C) for 12 h. The OTS-treated glass capillaries were then cut to 50 mm in length. Then, the OTS-coated glass capillaries were sonicated in ethanol and in water for 10 min each to remove unreacted OTS from the surface.

2.2 Formation of surface nanodroplets

Surface nanodroplets were formed inside the OTS-treated glass capillary tube using the solvent exchange process.[52] To deliver the solutions, the capillary tube was connected to a portable device composed of two shut-off valves joined with a T-junction (Fig. 1a).

The shut-off valves could prevent trapping of air during the sequential delivery of solutions A and B, guaranteeing mixing between the two to drive oversaturation of extractants and form the nanodroplets on the capillary tube wall.[52]

The droplets were generated according to the overall procedure shown in Fig. S1 in the ESI.† First, a solution of 5% octanol (Sigma Aldrich) in 50 vol% ethanol (Sigma Aldrich, reagent grade) aqueous solution (solution A) was injected into the glass capillary. At this point, only the outlet valve was open to let the solution flow to the capillary. Then, the syringe was removed from the device and pure water (solution B) was injected into the device using a new syringe. The air trapped during exchange of syringes could be removed by closing the outlet valve and opening the waste valve to block the passage of air to the capillary and flush it out to the side tube. After removing the air, the waste valve was again closed and the outlet valve was opened to let water into the capillary to displace solution A and generate the droplets, as shown by the three-dimensional confocal fluorescence image in Fig. 1a.

2.3 Nanoextraction of the analytes using surface nanodroplets

Target analytes were extracted from the solid suspension simply by injecting the suspension sample into the capillary tube with the nanodroplets on the wall. The solid particles in the suspension sample did not damage the nanodroplets during the extraction process due to the pinning effect from the capillary tube wall. After extraction, the analytes in the droplet could be observed *in situ* using fluorescence microscopy (Fig. 1b). When the analyte concentration is too high and interferes with the detection, it is possible to remove the excess suspension sample in the capillary tube simply by washing it away with water. However, this was not always necessary within the range of concentrations tested in this work.

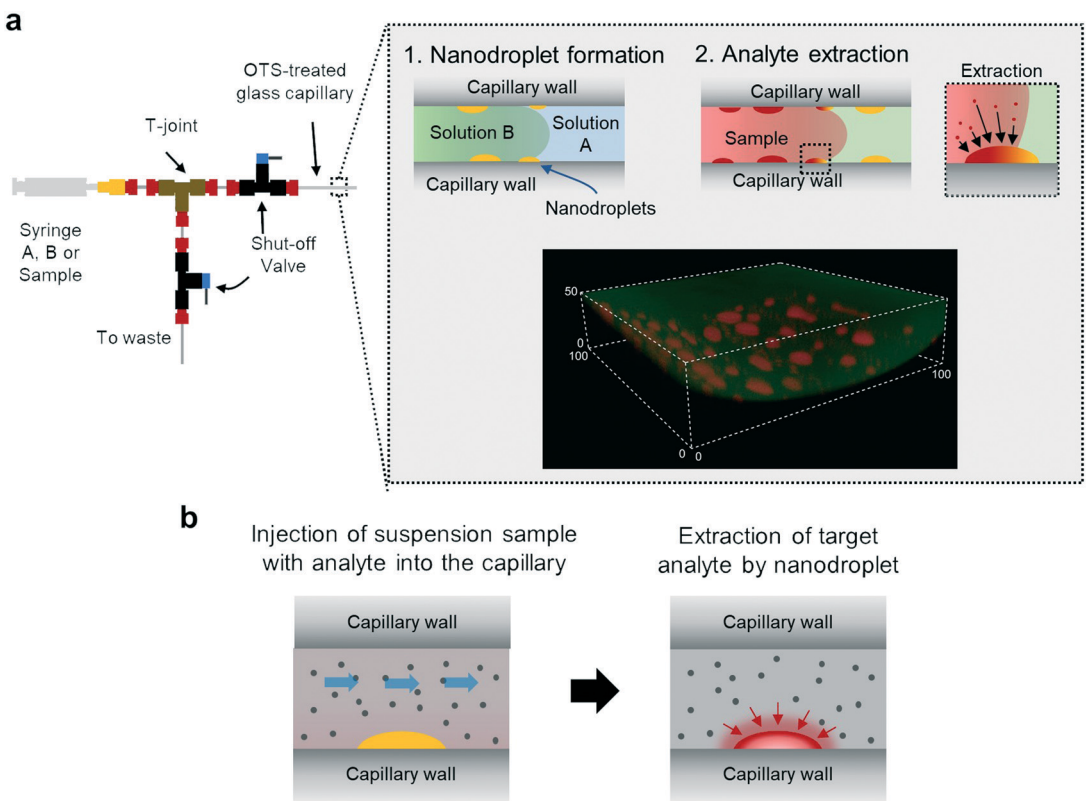

Fig. 1 Schematic diagram showing the surface nanodroplet formation and analyte detection using a portable solvent exchange device. a) The surface nanodroplets are formed on the inner wall of the OTS-treated glass capillary tube. For detection, the analyte-containing sample can be injected into the capillary tube decorated with surface nanodroplets, into which analytes were extracted. Inset: Confocal micrograph of surface nanodroplets formed on the inner wall of the glass capillary tube. b) Schematic showing the extraction of analytes from suspension samples. Extraction is simply achieved by flowing the sample through the capillary tube. As the slurry flows through the capillary tube, analytes are readily extracted into the surface nanodroplets.

2.4 Fluorescence detection of extracted analytes

The capillary tube was placed horizontally on the microscope and the fluorescence intensity of the droplets in the midway of the capillary tube was measured under green laser light to excite both Rhodamine B and Nile red. Unless otherwise noted, the exposure times were kept constant.

The intensity values of the droplets were analyzed using ImageJ. Intensity from individual droplets was analyzed rather than the total fluorescence intensity within a field of view because the number of droplets in a field of view cannot always be the same.

For the limit of detection tests, as the range of concentrations of the analyte in the suspension sample is large (covering three orders of magnitude), it was not possible to set an exposure time to measure the fluorescence signals of the droplets for all the cases. An exposure time set to detect the analyte concentration corresponding to 10^{-6} M was too short to analyze the droplets with lower concentrations such as 10^{-9} M. On the other hand, a selected exposure time appropriate to detect an analyte concentration of 10^{-9} M was too long for a concentration of 10^{-6} M and resulted in intensity saturation. Therefore, in order to determine the limit of detection, the images were acquired at different exposure times, and the intensity values were normalized to the value corresponding to 400 ms of exposure time. To avoid erroneous normalization, fluorescence intensities of the background were obtained at various exposure times for different concentrations within the linear region (Fig. S2 in the ESI†). All experiments shown in this work were repeated 3 times.

3 Results and discussion

3.1 Formation of the surface nanodroplets on the capillary wall for nanoextraction from solid suspensions

First, we demonstrate how the injection flow rate and the oil concentration influence the formation of the surface nanodroplets on the capillary tube wall. The optical images in Fig. 2a show that the droplets were similar in size and

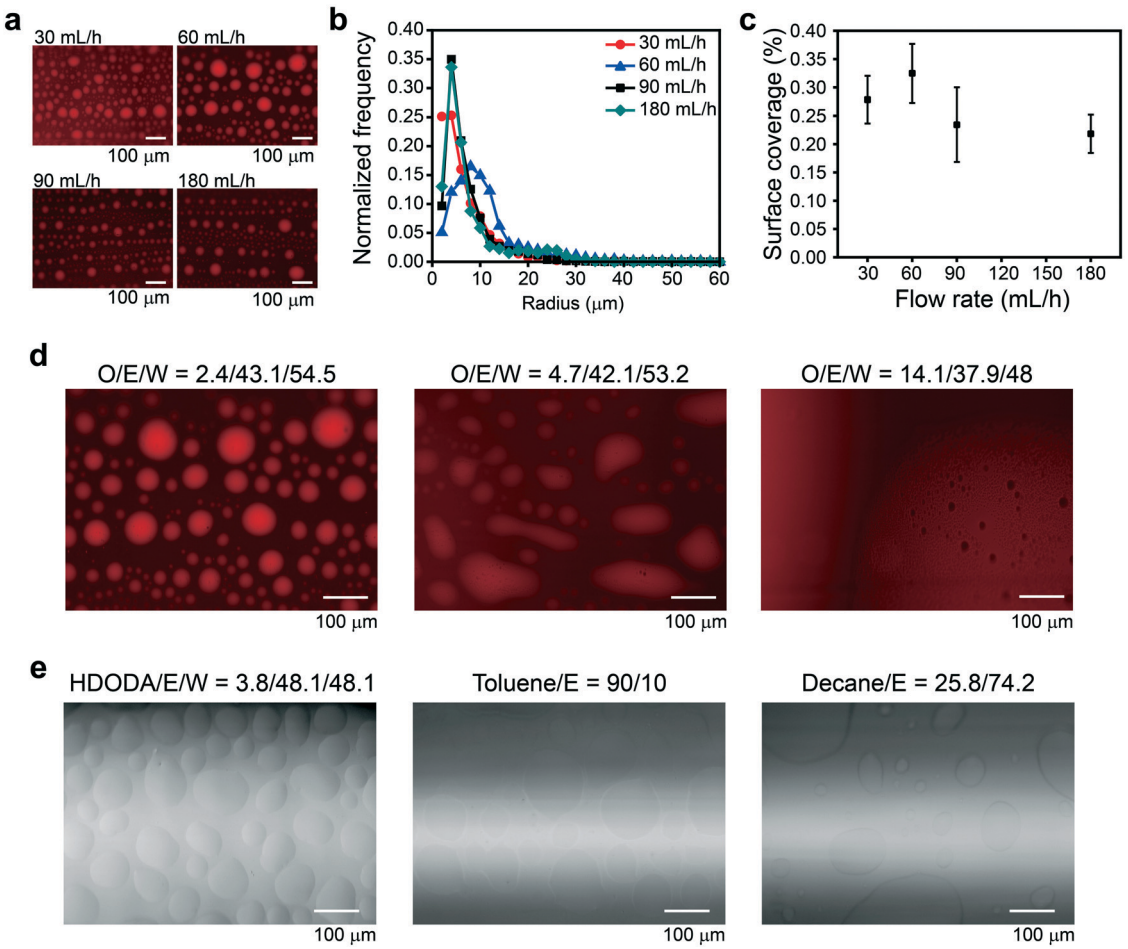

Fig. 2 The effect of the flow rate, oil concentration and oil type on the formation of surface nanodroplets in the glass capillary tube. a) Fluorescence images of the droplets formed with flow rates of 30, 60, 90 and 180 mL h^{-1} for solution B. b) Size distribution of the droplets formed under each flow rate condition. c) Surface coverage of the droplets formed under each flow rate condition (mean ± S.D.). d) Fluorescence images of the droplets formed at different solution A compositions (in wt%). e) Optical microscopy images of the droplets formed using different types of oils. The compositions are in wt%.

surface coverage on the wall, independent of the flow rate, which ranged from 30 to 180 mL h^{-1}. At the fastest flow rate, it took only ~20 s to form the surface nanodroplets on a 50 mm-long tube due to the small diameter and volume of the tube. The probability distribution function (PDF) plots in Fig. 2b show that most droplets were ~5 μm in base radius. The surface coverage (Fig. 2c) was between 20% and 35%, comparable to the value on a flat substrate with the same coating.[60] We attribute the independence of the droplet size distribution from the flow rate to the geometry confinement in a capillary tube. This is in contrast to the faster droplet growth at a faster flow demonstrated in a flow chamber with a flat substrate.[52]

An effective way to vary the droplet size is by simply changing the oil (*i.e.* octanol) concentration in solution A. Fig. 2d shows the fluorescence images of the droplets formed with octanol as the extractant. The flow rate was kept at 60 mL h^{-1} for all cases. As the concentration of octanol in solution A varied from 2.4 wt% to 4.7 wt%, the average base radius of the droplets increased from 10.9 μm to 14.3 μm. At an even higher concentration of 14.1 wt%, the droplets were too large, covering the field of view. Controlling the size is important for achieving high extraction efficiency as the droplet volume is known to influence the extraction performance.[61] The ratio between the droplet–water interfacial area and the droplet volume is critical in determining the rate of extraction. As it is explained in detail in the next section, the extraction rate increases with the decrease in droplet size.

The size and aspect ratio of the droplets can also be adjusted by adding surfactants in solution B, as demonstrated in our earlier work.[62] It was reported that when surfactants are present in solution B during solvent exchange, the droplet aspect ratio increases with surfactant concentration.[62] In this work, however, no surfactant was added in the solutions.

Surface nanodroplets can also be formed using many other types of extractants such as 1,6-hexanediol diacrylate (a type of monomer), toluene (aromatic solvent), and decane (alkane), as shown in the optical microscopy images in Fig. 2e. The selection of solution A and B in each case was guided by the solubility diagram of the extractant liquid, the good solvent, and the poor solvent. In the literature, solvent exchange has been applied for forming droplets of unconventional liquids such as extremely viscous silicone elastomers[63] or ionic liquids.[64] We expect that these droplets can be formed on capillary tubes as well since the principle of droplet nucleation and growth is the same regardless of chamber geometry. Formation of droplets with various extractant liquids expands the type of chemicals that can be extracted and analyzed, as extraction of certain analytes can depend on the extractant type.[65] Moreover, with a wider library of extractant liquids, the use of toxic and harmful extractants can be avoided.

Next, we demonstrate the capability of surface nanodroplets to extract analytes from solid suspensions. Nile red fluorescent dye at an initial concentration of 10^{-6} M was used as a model compound. The dye was dissolved in suspensions containing 3.125 mg mL^{-1} to 12.5 mg mL^{-1} of 150 nm silica particles. This range of nanoparticle concentration is similar to the solid contents in sewage sludge (10–1000 mg kg^{-1}).[66]

When the particle suspension was loaded into the capillary tube coated with the preformed surface nanodroplets, it was difficult to observe the droplets in the bright-field microscope image due to scattering of light by the particles (Fig. 3). However, in the fluorescence image, the droplets were clearly visible as the model analyte was readily extracted from the suspension into the droplets. The strong fluorescence intensity in the droplets indicates successful extraction of the dye (the target analyte) by the surface nanodroplets even in the presence of solid particles. In the following sections, we show the influence of the solid contents on the nanoextraction kinetics and detection sensitivity.

3.2 The effect of solid contents on nanoextraction kinetics

Next, we compare the nanoextraction kinetics in water and in a suspension sample. Fig. 4a shows the fluorescence images of the droplets after extracting the dye from an aqueous solution (left panel) and from a silica suspension (right

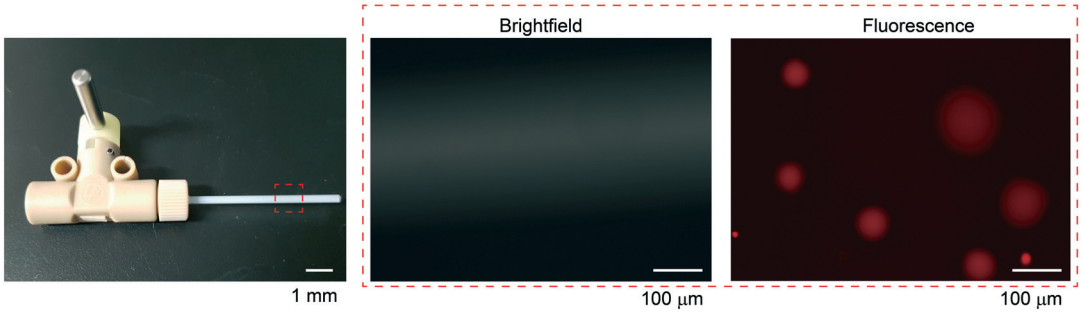

Fig. 3 Extraction of Nile red dye from the samples with various particle concentrations. Digital camera image of the glass capillary filled with silica solution (left). Bright field (center) and fluorescence images of the capillary tube (right). The droplets are not visible in bright field but are clearly shown in the fluorescence image due to the extraction of Nile red dye.

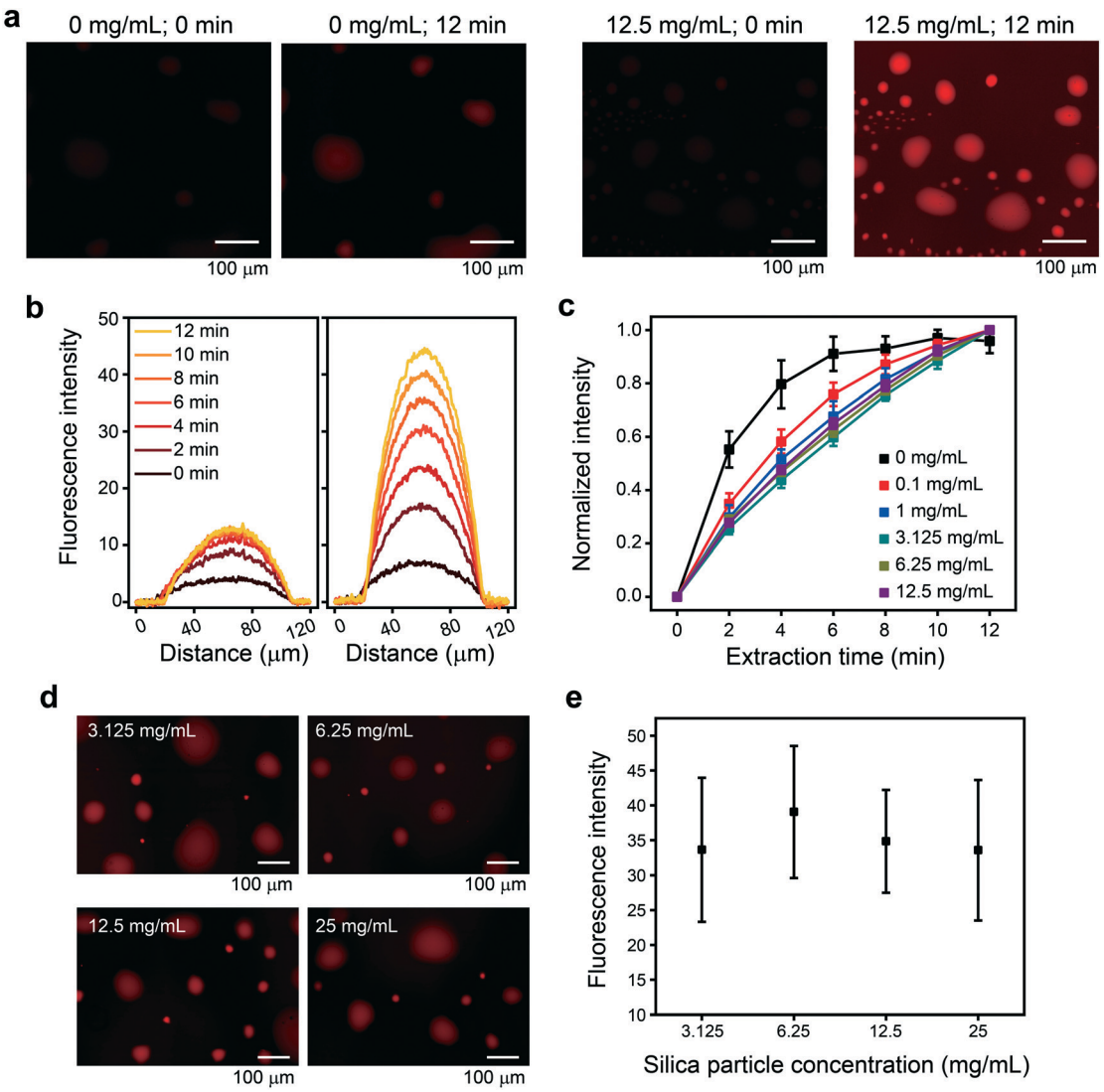

Fig. 4 The influence of solid particles on the extraction time. a) Fluorescence images of the droplets after extracting Nile red from the sample with no particle (0 mg mL^{-1}) and with particles (12.5 mg mL^{-1}). b) Intensity profiles across a droplet in the samples with and without particles. c) Comparison of normalized maximum intensities of the measured droplet over time. d) Fluorescence images and e) intensities of the droplets after extracting Nile red from the slurry solutions with particle concentrations of 3.125, 6.25, 12.5, and 25 mg mL^{-1}, respectively. Here, the Nile red concentration was 10^{-6} M for all cases. Error bars represent ±S.D.

panel) at a concentration of 12.5 mg mL^{-1}. The images at 0 min were acquired as soon as the sample was injected into the capillary tube. Fig. 4b shows the intensity profiles across a single droplet tracked over 12 min. It is clear that for the aqueous solution (*i.e.* 0 mg mL^{-1}), the profiles overlap from 6 min whereas those for the silica solution do not reach their maximum value even after 12 min.

When the normalized maximum intensity across the droplet was plotted against time (Fig. 4c), it was evident that the extraction time is delayed in the case of the suspension sample. The rate was distinguishable up to a particle concentration of 0.1 mg mL^{-1}, but no difference was observed at higher concentrations from 1 mg mL^{-1}. The slower extraction time in the case of the suspension sample may be attributed to hindered transport of analytes into the droplet due to the adsorbed silica particles at the droplet–water interface. Similar observations were reported by Goodarzi *et al.* from liquid–liquid extraction using a single oil droplet rising up a column of particle solutions.[67] Adsorption of small particles on an oil–water interface is well studied and widely used in the formation and stabilization of Pickering emulsions.[68] The contact angle of the particles at the interface and the interfacial energy between the two liquids (*i.e.* water and oil) determine how strongly a particle can adsorb to the interface.[69]

Although it has been reported that increased viscosity of a slurry can also reduce mass transfer during extraction,[70] this is unlikely the case since the silica concentration used here is not high enough to significantly influence the viscosity.

We can estimate the influence of solids on the extraction kinetics based on the theory established for single drop microextraction.[35] The concentration of the analyte extracted into the droplet (C_{drop}) is a function of time (t), concentration of the analyte in the sample (C_{aq}), partition coefficient (p), the ratio of free droplet interfacial area to droplet volume (A_{drop}/V_{drop}), and the mass transfer coefficient ($\bar{\beta}$) relating the diffusivity and concentration boundary layer thickness around the droplet,[61]

$$\frac{dC_{drop}}{dt} = \frac{A_{int}}{V_{drop}}\bar{\beta}\left(pC_{aq} - C_{drop}\right).$$

As the particles assemble on the droplet surface, the free droplet interfacial area (*i.e.* A_{drop}) decreases. With lower A_{drop} due to solid particle adsorption, the rate of increase of the analyte concentration in the droplet is slower. Assuming a surface coverage of 25%, it would require at least 3×10^9 particles to cover all the droplets, estimated using the size of individual particles (*i.e.* 150 nm). In a suspension with a concentration of 0.1 mg mL^{-1} particles, there are 1.3×10^9 particles available in the capillary, which is only ~40% of particles required to cover all the droplets. However, at a particle concentration of 1 mg mL^{-1} and above, the number of particles in the capillary is more than what is required for full droplet coverage (*i.e.* $\sim 1.2 \times 10^{10}$ particles for the case of 1 mg mL^{-1}). This is significantly higher than the required particle number to fully cover the droplets. Therefore, we can assume that all the droplets in the capillary are covered with the particles at concentrations higher than 1 mg mL^{-1}. This explains the slower extraction rate for suspension samples and the slight difference observed in the extraction rate for concentrations higher than 1 mg mL^{-1} in Fig. 4c. The reduction of the extraction rate is due to the fact that particle adsorption blocks the surface of the droplets for diffusion.

However, for a sufficiently long time (>30 min) of extraction, the signal intensities of the droplets eventually become independent of the particle concentration as shown in Fig. 4d. When tested with the particle concentration ranging from 3.125 to 25 mg mL^{-1}, the average fluorescence intensities of the droplets after extraction for more than 30 min were the same (Fig. 4e). This demonstrates that within the tested range, the amount of particles do not affect the efficiency of extraction. As the blocking effect from solid particles does not change the partition coefficient, the concentration of the analyte in the droplet liquid in equilibrium with the suspension does not depend on the solid concentration. Therefore, after a sufficiently long time, the analyte concentration in the droplets reached the same level, independent of the solid contents. Extraction may be

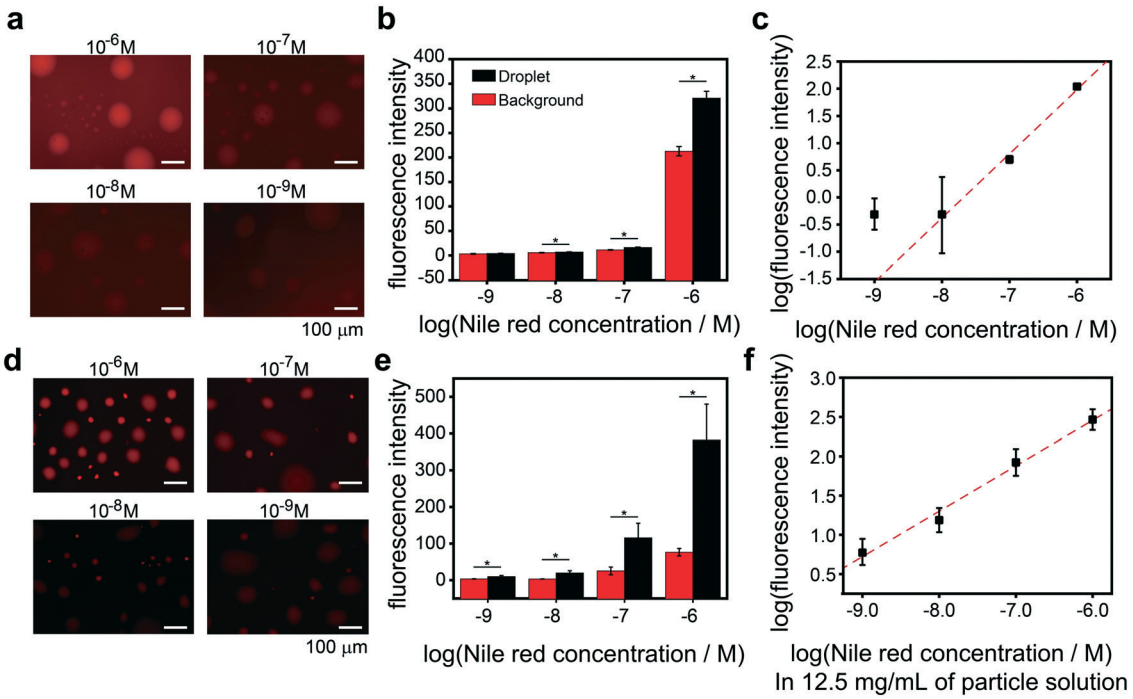

Fig. 5 Limit of detection and low sample volume requirement of the portable nanoextraction device. a) Fluorescence images of the surface nanodroplets after extracting Nile red from water with different initial concentrations. b) Average fluorescence intensity values of the surface nanodroplets and the background after the extraction of Nile red from water. Here, * indicates $p < 0.05$. c) Fluorescence intensity of the droplets after subtracting the background signal. The slope in this log–log plot is ~1.2. The outlier point indicates that the limit of detection for Nile red is 10^{-9} M. d) Fluorescence images of the surface nanodroplets after extracting Nile red from silica solution (12.5 mg mL^{-1}) with different initial concentrations. e) Average fluorescence intensity values of the surface nanodroplets and the background after the extraction of Nile red from water. Here, * indicates $p < 0.05$. f) Fluorescence intensity of the droplets after subtracting the background signal. The slope of the log–log plot is ~0.6.

influenced if the analytes and solid content in the sample interact with each other such as in the case of adsorption of chemicals onto micro/nanoplastics *via* hydrophobic and electrostatic interactions.[71,72]

3.3 Extraction performance and sensitivity of nanoextraction from solid suspensions

Fig. 5a shows the fluorescence images of the octanol surface nanodroplets after extracting Nile red dyes from particle-free aqueous solutions in an initial concentration range between 10^{-6} M and 10^{-9} M. Nile red has an octanol–water partition coefficient of $\log P \sim 5$ so the concentration of the dye in octanol is ~100 000× that of water in equilibrium.[73] As a result, after extraction, the droplets can be clearly differentiated from the background, owing to the higher concentration of the analyte.

Quantification of the fluorescence intensities in the droplets and background aqueous solution demonstrates that the limit of detection for the Nile red dye from aqueous solution is 10^{-8} M. Fig. 5b shows the average fluorescence intensity of the droplets and background aqueous solution measured in the vicinity of each corresponding droplet. The intensity in the droplet is higher for the initial Nile red concentration range of 10^{-6} M to 10^{-8} M with a statistical significance of $p < 0.05$. However, at the dye concentration of 10^{-9} M, no difference between the droplets and background suspension was observed. Taking the logarithm of the difference between the average intensity values of the droplets and of the background aqueous solution yields a calibration curve in log–log scale, correlating the fluorescence intensity and the initial dye concentration (Fig. 5c), with a power law dependence with an effective scaling exponent of ~1.2 in the range of initial concentrations between 10^{-6} M and 10^{-8} M, which is the limit of detection.

The limit of detection depends on factors such as the partition coefficient and the quantum efficiency of the fluorescent dyes. We compared it to another model compound – Rhodamine B, which has a lower partition coefficient as compared to Nile red ($\log P \sim 2.3$ *vs.* $\log P \sim 5$).[58] With Rhodamine B, the limit of detection was lower (*i.e.* 10^{-9} M) as compared to Nile red (Fig. S3†), possibly due to its comparatively higher quantum efficiency.[74]

In the same way, the limit of detection for a suspension sample with 12.5 mg mL^{-1} of 150 nm silica particles was tested using Nile red as the model compound. The initial concentration of Nile red in the silica solutions varied from 10^{-6} M to 10^{-9} M. Fig. 5d shows the fluorescence images of the droplets after the extraction of Nile red from the silica solutions. Again, the droplets can clearly be distinguished from the background suspension solution. The average fluorescence intensities of the droplets are statistically higher compared to that of the background, down to an initial Nile red concentration of 10^{-9} M, which is an order of magnitude lower than that in the aqueous solution. The calibration curve in log–log scale obtained from the difference in the droplet and background intensities reveals a power law, but with a lower effective scaling exponent of ~0.6. The lower limit of detection and lower effective scaling exponent in the calibration curve may be due to the interaction of Nile red molecules at the particle–water interface.

The advantageous high fluorescence intensity in the suspension samples compared to that in the aqueous samples may be attributed to the synergistic effect of 1) the interaction of Nile red molecules with the silica nanoparticles and 2) the adsorption of silica nanoparticles to the droplet–water interface. It is likely that Nile red molecules adsorb on the nanoparticle surface and then adsorb at the droplet–water interface influencing the fluorescence intensity change with the Nile red concentration in the sample. For the samples without any particles, the fluorescence intensity change with the Nile red concentration is mainly due to the partitioning of Nile red into the surface nanodroplets. However, in the case of silica nanoparticles, the increase in fluorescence intensity is attributed to both partitioning of Nile red and adsorption of Nile red-bound silica nanoparticles. The effect from adsorbed particles on the fluorescence intensity may also explain why the slope shown in Fig. 5c is steeper than that shown in Fig. 5f. Fig. 6 shows a plot of the fluorescence intensity of the droplets and the total surface area of particles corresponding to the concentration range between 3.125 mg mL^{-1} and 12.5 mg mL^{-1}. The total surface area of particles was calculated by multiplying the surface area of a single 150 nm particle (density ~ 2 g cm^{-3}) with the total number of particles available in the capillary tube (volume ~ 48 μL), which is determined by the particle concentration in the suspension. At a higher particle concentration, there is more area available for the analyte molecules to be adsorbed on such that with more particles adsorbed at the droplet–water interface, more analyte is available as well to increase the fluorescence signal.

At extremely low concentrations, the location along the capillary tube where the fluorescence signal is measured may

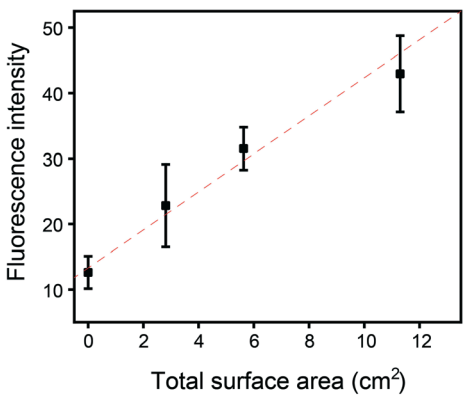

Fig. 6 Plot showing the relationship between the intensity of the droplet and the total surface area offered by the particles. The total surface area of the particles was calculated by multiplying the surface area of a 150 nm particle with the total number of the particles available in the capillary tube.

influence the detection sensitivity. As the sample flows through the tube, the target compounds are continuously extracted by the surface nanodroplets downstream and the total amount of the compounds decreases due to extraction upstream. Therefore, if the concentration is low enough, the fluorescence intensity in the droplets could be lower towards the outlet of the capillary tube. However, at the tested concentrations, no difference in the signal intensities was observed along the capillary tube as the field of view is further from the outlet.

3.4 The influence of sample volume on extraction performance

Apart from simplicity and high efficiency, another crucial advantageous feature of nanoextraction is the small sample volume (on the order of μL), thanks to the confined geometry of the glass capillary. As shown in Fig. 7a and b, the detection of Nile red (concentration = 10^{-6} M) can be performed with sample volumes as low as 50 μL. Fluorescence intensity of both the droplets and background remained unchanged down to 50 μL (Fig. 7b). As a result, the difference between the signal from the droplet and that from the background is also similar for the same range of sample volumes (Fig. 7c), demonstrating reliable extraction.

The reason that reliable extraction is observed with a volume as low as 50 μL is attributed to the volume of the capillary, which is ~48 μL (i.d. = 1.1 mm and length = 50 mm). When the sample is introduced to the capillary, it can completely replace solution B and the droplets can extract the target analytes. On the other hand, in the case of 25 μL volume, the sample does not thoroughly replace the solution contained in droplet B such that the fluorescence intensity is very low when imaged with the same exposure time.

In addition, the fact that the surface nanodroplets are on the scale of femtoliters plays a significant role in lowering the required sample volume.[57] Liquid–liquid extraction relies on the partition coefficient ($\log P$) of the analytes which is determined by the concentration of the analytes in the sample and the extractant oil at equilibrium. Thus, even if the sample volume is low, the volumes of the surface nanodroplets can still be much lower than those of the sample, enabling reliable extraction.

Extraction of analytes from a low sample volume is of high interest in many diagnostic applications involving body fluids such as saliva[75,76] or blood.[77] However, in conventional extraction methods such as DLLME or single-drop microextraction, the sample volume is usually increased by diluting the sample with water prior to extraction. In doing so, the concentration of the analyte in the sample decreases, reducing the sensitivity. Moreover, many of the commonly used microextraction processes that employ centrifugation are challenged by the difficulty of separating the centrifuged oil pellet from the sample if the sample volume is low.

3.5 Extraction of the target analyte from oil sand wastewater

The portability of the entire device is potentially useful for analysis in the field such as in environmental monitoring. As a proof-of-concept demonstration, we show the extraction of the target analyte from oil sand wastewater comprising of solid particles, bitumen (heavy oil) and other hazardous hydrocarbons such as naphthenic acids or adamantane.[78] Detection of such analytes from oil sand wastewater is important for the environment as seepage of these chemicals into the ground or surface water can cause adverse effects on the aquatic life.[78]

In Fig. 8a, we show the extraction of Nile red from an oil sand wastewater sample comprising of 0.1 wt% bitumen, 7 wt% solids (fine and sand) and 92.9 wt% water. Prior to extraction, Nile red – mimicking hydrophobic compounds in the wastewater – was added to the oil sand wastewater sample at concentrations ranging from 10^{-6} M to 10^{-9} M. Similar to the extraction from a silica suspension, we determined the limit of detection for the oil sand wastewater sample based on the fluorescence intensity in the droplet and in the background. The limit of detection was 10^{-8} M, an order of magnitude lower than that of the silica solution as

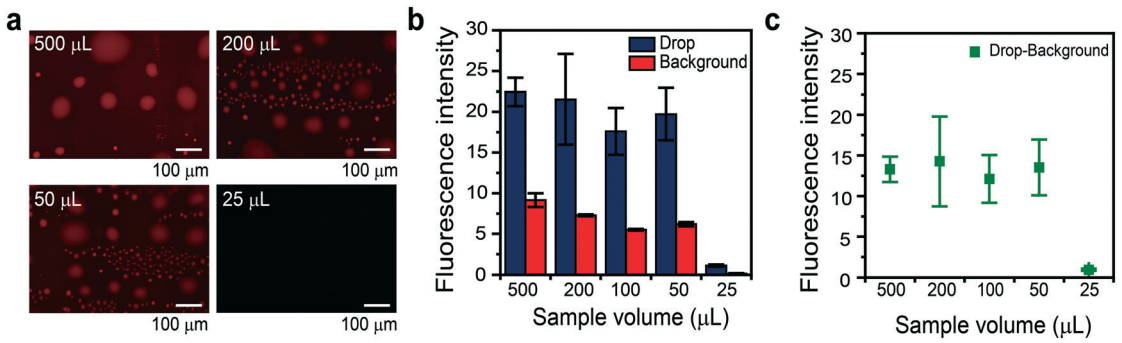

Fig. 7 Processing of the sample at low volumes. a) Fluorescence images of the surface nanodroplets after extracting a 1 μM aqueous solution of Nile red at different sample volumes. For better visualization purposes, the brightness has been adjusted. b) Fluorescence intensity values of the nanodroplets and background after the extraction of 10^{-6} M Rhodamine B solution. c) Fluorescence intensity of the droplets after subtracting the background signal. The intensity values for various sample volumes are similar from 500 μL to 50 μL, but the signal is negligible at the sample volume of 25 μL.

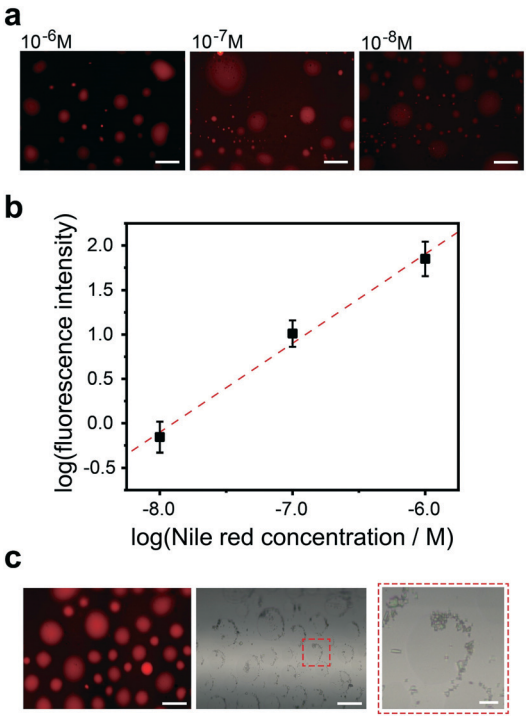

Fig. 8 Extraction of the analyte from the complex oil sand wastewater sample. a) Fluorescence images of the oil sand wastewater with Nile red at 10^{-6} M to 10^{-8} M. b) Limit of detection for the Nile red in the oil sand wastewater sample. When plotted in log–log scale, a linear trend is observed, *i.e.* the slope is ~1. c) Extraction of 10^{-6} M Nile red dye from the oil sand wastewater with a high solid content (~30 wt%). The dye is readily extracted into the droplets. However, the presence of particle aggregates is observed at the droplet–water interface.

shown in Fig. 8b. The lower detection sensitivity from the oil sand wastewater may be attributed to the sorption of Nile red molecules to the solid particles that are potentially fouled by bitumen. As bitumen is known to be an aggressive foulant,[79] it is possible for solid particles to have bitumen coating the surface. Then, Nile red can be adsorbed on the bitumen-coated solids thereby lowering the liquid–liquid extraction efficiency by the surface nanodroplets.

Nonetheless, the extraction was successful even with an oil sand wastewater sample with a higher solid content of ~30 wt% as shown in Fig. 8c. The sample was spiked with 10^{-6} M of Nile red dye and it was injected into the capillary device after forming surface nanodroplets with octanol. The Nile red dye was readily extracted into the droplets from which a strong fluorescence signal was detectable. Although some particles aggregated at the droplet–water interface due to their excessive amount in the sample, their influence would be minimal on the detection of extracted analytes in the droplets by *in situ* methods.

4 Conclusion

In summary, we developed a green and sustainable nanoextraction approach for concentrating compounds from highly concentrated solid suspensions using surface nanodroplets. Extraction of model analytes was feasible for suspension samples with a solid content of up to 30 wt%. Without prior removal of solids, nanoextraction is fast, requiring only sub-milliliter sample volume. As a proof-of-concept, a target compound was extracted from an oil–sand slurry. A similar limit of detection was observed for both aqueous samples and suspension samples (10^{-8} M and 10^{-9} M), demonstrating that particles do not reduce the extraction efficiency for the target analytes. Instead, the particles initially slowed down the extraction rate due to their adsorption to the droplets.

In future work, the extracted analytes can be analyzed using other *in situ* methods such as UV-vis microspectrophotometry, surface-enhanced Raman spectroscopy, or attenuated total reflection (ATR) infrared spectroscopy. We expect that the technology shown in this work provides opportunities to rapidly and easily separate target analytes from complex samples in low volumes such as saliva or blood, which will be useful for diagnostic applications, or for online analysis of slurries in the environment.

Conflicts of interest

There are no conflicts to declare.

Acknowledgements

This project was supported by the ERC Proof-of-Concept grant (Project Number 862032). The project was also partly supported by the Natural Science and Engineering Research Council of Canada (NSERC) and the Future Energy Systems (Canada First Research Excellence Fund). XZ acknowledges support from the Canada Research Chairs Program.

Notes and references

1 M. Tobiszewski, A. Mechlińska, B. Zygmunt and J. Namieśnik, *TrAC, Trends Anal. Chem.*, 2009, **28**, 943–951.
2 M. Tobiszewski, *Anal. Methods*, 2016, **8**, 2993–2999.
3 M. Llompart, M. Celeiro, C. García-Jares and T. Dagnac, *TrAC, Trends Anal. Chem.*, 2019, **112**, 1–12.
4 S. Tosi, M. Rossi, E. Tamburini, G. Vaccari, A. Amaretti and D. Matteuzzi, *Biotechnol. Prog.*, 2003, **19**, 1816–1821.
5 C. Quintelas, A. Braga, D. P. Mesquita, A. L. Amaral, E. C. Ferreira and I. Belo, *J. Chem. Technol. Biotechnol.*, 2019, **94**, 812–818.
6 D. Brassard, M. Geissler, M. Descarreaux, D. Tremblay, J. Daoud, L. Clime, M. Mounier, D. Charlebois and T. Veres, *Lab Chip*, 2019, **19**, 1941–1952.
7 H. Tabani, A. Shokri, S. Tizro, S. Nojavan, P. Varanusupakul and M. Alexovič, *Talanta*, 2019, **199**, 329–335.
8 H. A. Mashayekhi, P. Abroomand-Azar, M. Saber-Tehrani and S. W. Husain, *Chromatographia*, 2010, **71**, 517–521.
9 Y. Choi, Y. T. Kim, J. B. You, S. H. Jo, S. J. Lee, S. G. Im and K. G. Lee, *Food Chem.*, 2019, **270**, 445–451.

10 Y. Zhang, X. Zhang and B. Jiao, *Food Chem.*, 2014, **159**, 367–373.
11 K. L. Soares, M. B. R. Cerqueira, S. S. Caldas and E. G. Primel, *Chemosphere*, 2017, **182**, 547–554.
12 P. J. Ducrest, S. Pfammatter, D. Stephan, G. Vogel, P. Thibault and B. Schnyder, *Sci. Rep.*, 2019, **9**, 5814.
13 M. Ren, H. Xu, X. Huang, M. Kuang, Y. Xiong, H. Xu, Y. Xu, H. Chen and A. Wang, *ACS Appl. Mater. Interfaces*, 2014, **6**, 14215–14222.
14 W. Boonjob, J. B. Quintana, R. Rodil, R. Cela and M. Miró, *Anal. Bioanal. Chem.*, 2013, **405**, 8653–8662.
15 A. Gałuszka, Z. Migaszewski and J. Namieśnik, *TrAC, Trends Anal. Chem.*, 2013, **50**, 78–84.
16 A. Braun, O. Couteau, K. Franks, V. Kestens, G. Roebben, A. Lamberty and T. P. J. Linsinger, *Adv. Powder Technol.*, 2011, **22**, 766–770.
17 L. Hildebrandt, D. M. Mitrano, T. Zimmermann and D. Pröfrock, *Front. Environ. Sci.*, 2020, **8**, 89.
18 Y. Wang, M. Huo, Q. Li, W. Fan, J. Yang and X. Cui, *J. Soils Sediments*, 2018, **18**, 2980–2994.
19 F. Springer, S. Laborie and C. Guigui, *Sep. Purif. Technol.*, 2013, **108**, 6–14.
20 Y. Kiso, Y. Nishimura, T. Kitao and K. Nishimura, *J. Membr. Sci.*, 2000, **171**, 229–237.
21 D. S. Doulia, E. K. Anagnos, K. S. Liapis and D. A. Klimentzos, *J. Hazard. Mater.*, 2016, **317**, 135–146.
22 M. Carlson and R. D. Thompson, *J. Chromatogr. Sci.*, 2000, 77–83.
23 S. Lath, E. R. Knight, D. A. Navarro, R. S. Kookana and M. J. McLaughlin, *Chemosphere*, 2019, 671–678.
24 R. Ahmad, R. S. Kookana and A. M. Alston, *Bull. Environ. Contam. Toxicol.*, 2001, 313–318.
25 A. Sarafraz-Yazdi and A. Amiri, *TrAC, Trends Anal. Chem.*, 2010, **29**, 1–14.
26 S. Tang, H. Zhang and H. K. Lee, *Anal. Chem.*, 2016, **88**, 228–249.
27 F. A. Hansen, H. Jensen and S. Pederson-Bjergaard, *Anal. Chem.*, 2020, **92**, 5595–5603.
28 C. Yeh, P. Cheng and S. Y. Chang, *Talanta*, 2019, **199**, 296–302.
29 F. Zarghampour, Y. Yamini, M. Baharfar, G. Javadian and M. Faraji, *Anal. Methods*, 2020, **12**, 483–490.
30 S. Pederson-Bjergaard and K. E. Rasmussen, *Anal. Chem.*, 1999, **71**, 2650–2656.
31 H. Y. Kaw, J. Li, X. Jin, Z. Wang, L. Cong, M. He and D. Li, *Analyst*, 2018, **143**, 4575–4584.
32 W. Bi, M. Tian and K. H. Row, *Talanta*, 2011, **85**, 701–706.
33 C. Bendicho, I. Costas-Mora, V. Romero and I. Lavilla, *TrAC, Trends Anal. Chem.*, 2015, **68**, 78–87.
34 J. Feng, M. Sun, H. Liu, J. Li, X. Liu and S. Jiang, *J. Chromatogr. A*, 2010, **1217**, 8079–8086.
35 M. A. Jeannot and F. F. Cantwell, *Anal. Chem.*, 1996, **68**, 2236–2240.
36 S. Tang, T. Qi, P. D. Ansah, J. C. N. Fouemina, W. Shen, C. Basheer and H. K. Lee, *TrAC, Trends Anal. Chem.*, 2018, **108**, 306–313.
37 D. B. G. Williams, M. J. George, R. Meyer and L. Marjanovic, *Anal. Chem.*, 2011, **83**, 6713–6716.
38 L. Guo, N. B. Nawi and H. K. Lee, *Anal. Chem.*, 2016, **88**, 8409–8414.
39 S. Zaruba, A. B. Vishnikin, J. Škrlíková and V. Andruch, *Anal. Chem.*, 2016, **88**, 10296–10300.
40 S. Zaruba, A. B. Vishnikin, J. Škrlíková, A. Diuzheva, I. Ozimaničová, K. Gavazov and V. Andruch, *RSC Adv.*, 2017, **7**, 29421–29427.
41 H. S. N. Lee, C. Basheer and H. K. Lee, *J. Chromatogr. A*, 2006, **1124**, 91–96.
42 C. Basheer and H. K. Lee, *J. Chromatogr. A*, 2004, **1047**, 189–194.
43 N. Reyes-Garcés, E. Gionfriddo, G. A. Gómez-Ríos, M. N. Alam, E. Boyaci, B. Bojko, V. Singh, J. Grandy and J. Pawliszyn, *Anal. Chem.*, 2018, **90**, 302–360.
44 S. Boonchiangma, W. Ngeontae and S. Srijaranai, *Talanta*, 2012, **88**, 209–215.
45 P. Viñas, N. Campillo, I. López-García and M. Hernández-Córdoba, *Anal. Bioanal. Chem.*, 2014, **406**, 2067–2099.
46 M. H. Habibollahi, K. Karimyan, H. Arfaeinia, N. Mirzaei, Y. Safari, R. Akramipour, H. Sharafi and N. Fattahi, *J. Sci. Food Agric.*, 2019, **99**, 656–665.
47 G. Özzeybek, S. Erarpat, D. S. Chormey, M. Firat, C. Büyükpinar, F. Turak and S. Bakirdere, *Microchem. J.*, 2017, **132**, 406–410.
48 M. Rezaee, Y. Assadi, M. R. M. Hosseini, E. Aghaee, F. Ahmadi and B. S, *J. Chromatogr. A*, 2006, **1116**, 1–9.
49 Q. Luo, S. Wang, M. Adeel, Y. Shan, H. Wang and L. Sun, *Sci. Rep.*, 2019, **9**, 11292.
50 C. B. Ojeda and F. S. Rojas, *Chromatographia*, 2018, **81**, 89–103.
51 D. Lohse and X. Zhang, *Rev. Mod. Phys.*, 2015, **87**, 981–1035.
52 X. Zhang, Z. Lu, H. Tan, L. Bao, Y. He, C. Sun and D. Lohse, *Proc. Natl. Acad. Sci. U. S. A.*, 2015, **112**, 9253–9257.
53 Z. Wei, M. Li, H. Zeng and X. Zhang, *Anal. Chem.*, 2020, **92**, 12442–12450.
54 J. Meng, J. B. You and X. Zhang, *J. Phys. Chem. C*, 2020, **124**, 12476–12484.
55 H. Yu, S. Maheshwari, J. Zhu, D. Lohse and X. Zhang, *Lab Chip*, 2017, **17**, 1496–1504.
56 D. Lohse and X. Zhang, *Nat. Rev. Phys.*, 2020, **6**, 426–443.
57 M. Li, B. Dyett, H. Yu, V. Bansal and X. Zhang, *Small*, 2019, **15**, 1804683.
58 M. Li, B. Dyett and X. Zhang, *Anal. Chem.*, 2019, **91**, 10371–10375.
59 R. Zhang, W. Liao, Y. Sun, J. Y. Y. Heng and Z. Yang, *J. Phys. Chem. C*, 2019, **123**, 1151–1159.
60 C. Xu, H. Yu, S. Peng, Z. Lu, L. Lei, D. Lohse and X. Zhang, *Soft Matter*, 2017, **13**, 937–944.
61 M. A. Jeannot and F. F. Cantwell, *Anal. Chem.*, 1997, **69**, 235–239.
62 H. Yang, S. Peng, X. Hao, T. A. Smith, G. G. Qiao and X. Zhang, *Soft Matter*, 2014, **10**, 957–964.
63 B. Dyett, H. Yu and X. Zhang, *Eur. Phys. J. E: Soft Matter Biol. Phys.*, 2017, **40**, 26.

64 H. Yu, B. P. Dyett, S. K. Pathirannahalage, M. Li, C. J. Drummond and T. L. Greaves, *Adv. Mater. Interfaces*, 2020, **7**, 1901647.
65 X. Wang, Y. Wang, X. Zou and Y. Cao, *Anal. Methods*, 2014, **6**, 2384–2389.
66 B. Kim, M. Murayama, B. P. Colman and M. F. Hochella Jr., *J. Environ. Monit.*, 2012, **14**, 1129–1137.
67 H. H. Goodarzi and M. N. Esfahany, *Sep. Purif. Technol.*, 2016, **170**, 130–137.
68 Y. Chevalier and M.-A. Bolzinger, *Colloids Surf., A*, 2013, **439**, 23–34.
69 B. P. Binks, *Curr. Opin. Colloid Interface Sci.*, 2002, **7**, 21–41.
70 S. W. Park, B. S. Choi, S. S. Kim, B. D. Lee and J. W. Lee, *J. Ind. Eng. Chem.*, 2008, **14**, 166–174.
71 P. S. Tourinho, V. Kočí, S. Loureiro and C. A. M. van Gestel, *Environ. Pollut.*, 2019, **252**, 1246–1256.
72 I. Velzeboer, C. A. J. F. Kwadijk and A. A. Koelmans, *Environ. Sci. Technol.*, 2014, **48**, 4869–4876.
73 F. Rashid-Doubell and R. W. Horobin, in *Biotechnology Applications of Microinjection, Microscopic Imaging, and Fluorescence*, ed. P. H. Bach, C. H. Reynolds, J. M. Clark, J. Mottley and P. L. Poole, Springer, London, 1993, p. 75.
74 N. Ghoneim, *Spectrochim. Acta, Part A*, 2000, **56**, 1003–1010.
75 A. Jouyban, M. A. Farajzadeh, M. Khoubnasabjafari, V. Jouyban-Gharamaleki, M. Reza and A. Mogaddam, *Anal. Methods*, 2019, **11**, 1530–1540.
76 I. Timofeeva, K. Medinskaia, L. Nikolaeva, D. Kirsanov and A. Bulatov, *Talanta*, 2016, **150**, 655–660.
77 S. Odoardi, M. Fisichella, F. S. Romolo and S. Strano-Rossi, *J. Chromatogr., B*, 2015, **1000**, 57–68.
78 L. M. Hewitt, J. W. Roy, S. J. Rowland, G. Bickerton, A. DeSilva, J. V. Headley, C. B. Milestone, A. G. Scarlett, S. Brown, C. Spencer, C. E. West, K. M. Peru, L. Grapentine, J. M. E. Ahad, H. Pakdel and R. A. Frank, *Environ. Sci. Technol.*, 2020, **54**, 1522–1532.
79 Q. Chen, J. Liu, T. Thundat, M. R. Gray and Q. Liu, *Fuel*, 2017, **191**, 283–289.